Contribution from the Departments of Chemistry, Tulane University, New Orleans, Louisiana 70118, and The University of Alabama, University, Alabama 35486

Electron Paramagnetic Resonance Studies of Manganese(II) and Nickel(II) in Three Structural Phases of Rubidium Magnesium Chloride and the Crystal Structure of 6H-Rubidium Magnesium Chloride

KENNETH O. DEVANEY,[1a] MARC R. FREEDMAN,[1a] GARY L. McPHERSON,*[1a] and JERRY L. ATWOOD*[1b]

Received November 2, 1979

Undoped $RbMgCl_3$ crystallizes in a hexagonal lattice, 6H, in which there are two crystallographically distinct magnesium ions. A complete X-ray analysis indicates that the structure is very similar to that of $CsCdCl_3$. Both magnesium ions are surrounded by approximately octahedral arrays of chloride ions. When a small concentration of Ni(II) (0.4–0.8 mol %) is present, $RbMgCl_3$ crystallizes in a different hexagonal lattice, 4H, which contains only one type of magnesium ion. If a greater concentration of Ni(II) (~4 mol %) is introduced, a third hexagonal lattice, 9R, results. The lattice constants indicate that this material has a structure similar to that of $CsMnCl_3$. There are two distinct types of divalent metal sites in this structure. The EPR spectra of $RbMgCl_3$ crystals doped with Mn(II) indicate that the manganese readily substitutes for magnesium in all three structural phases. The Mn(II) resonances can be accurately described by an axial spin Hamiltonian and can be assigned to particular sites in the host materials. The Ni(II) resonance in 4H-$RbMgCl_3$ (0.4–0.8 mol % Ni(II)) can also be described by an axial spin Hamiltonian.

Introduction

Double salts of the formula AMX_3 (where A is a monovalent cation, M a divalent metal ion, and X a halide) have been shown to crystallize in a number of distinct lattice types. In general the lattices can be described as infinite arrays of MX_6^{4-} octahedra joined at either corners or faces. The lattice types are distinguished by the manner in which the octahedral complexes connect to form the infinite array. Schematic diagrams of the various lattice types exhibited by the AMX_3 salts are shown in Figure 1. Of these, the perovskite, 3C, and the $CsNiCl_3$ type, 2H, can be thought of as structural extremes. The perovskite consists of octahedra joined only at corners to give a three-dimensional network while $CsNiCl_3$ consists of octahedra joined only at faces which produces infinite linear chains. The other lattice types contain both corner- and face-shared octahedra. The factors determining which of the lattice types a given AMX_3 salt will adopt have been considered in some detail by Schippers and co-workers.[2] Longo and co-workers have shown that application of high pressure to certain AMX_3 salts causes structural transitions from one lattice type to another.[3-6] In some cases, several distinct transitions are observed as the pressure is increased. It appears, for particular AMX_3 salts that the thermodynamic stabilities of the various lattice types are not dramatically different.

The concept of several structures with very similar stabilities seems particularly appropriate for the magnesium salt $RbMgCl_3$. Tishura and co-workers reported $RbMgCl_3$ to be isostructural with $CsMgCl_3$ which is a 2H-type lattice.[7] Seifert and Fink presented a complete X-ray study showing that the salt adopts a 4H lattice.[8] Diffraction studies of $RbMgCl_3$ prepared in our laboratories indicate that the material has the 6H structure of $CsCdCl_3$ and $RbMnCl_3$. Presumably, the $RbMgCl_3$ was prepared by the same method in each case (fusion of equimolar mixtures of RbCl and $MgCl_2$). For a simple salt, the apparent structural variation exhibited by $RbMgCl_3$ seems unusual.

As part of a general study of the spectroscopic properties of transition-metal ions in AMX_3 salts, crystals of $RbMgCl_3$ doped with divalent ions such as Mn(II) and Ni(II) were grown and characterized. In the course of the studies it became apparent that small concentrations of Ni(II), as little as 0.4 mol %, produce changes in the structure of the host material. The lattice constants of $RbMgCl_3$ crystals containing 0.4–0.8 mol % Ni(II) are not consistent with the $CsCdCl_3$ structure. The unit cell dimensions of these doped crystals are nearly identical with those of the $RbMgCl_3$ crystals prepared and characterized by Seifert and Fink. If a greater concentration of Ni(II) is present in $RbMgCl_3$ (~4 mol %), a third structural phase is obtained. The lattice constants of this material are consistent with a 9R structure like that of $CsMnCl_3$. The following designations have been adopted for the three structural phases: 6H-$RbMgCl_3$, 4H-$RbMgCl_3$, and 9R-$RbMgCl_3$. It is recognized that crystals of 9R-$RbMgCl_3$ contain an appreciable concentration of Ni(II). A more exact formulation would be $RbMg_{0.96}Ni_{0.04}Cl_3$. In contrast with Ni(II), small concentrations of Mn(II) do not appear to be an important factor in determining which of the lattice types is adopted by $RbMgCl_3$. The EPR spectra of the doped crystals indicate that the manganese impurities randomly replace the magnesium ions in the lattice regardless of which structure is assumed by the host material. It is possible to observe a Mn(II) spectrum in all three structural phases of $RbMgCl_3$. This paper presents a complete crystal structure determination of 6H-$RbMgCl_3$, an analysis of the EPR spectra of $RbMgCl_3$ crystals doped with Mn(II) and Ni(II), and a discussion of the unusual structural chemistry of $RbMgCl_3$.

Experimental Section

Preparation of Materials. The pure $RbMgCl_3$ salt was prepared by fusing equimolar amounts of RbCl (ultrapure, Alfa Chemicals) and $MgCl_2$ (anhydrous, purified by zone refinement) under vacuum at approximately 650 °C. The colorless crystalline solid is very hygroscopic and must be handled in a dry atmosphere. All manipulations were carried out in a dry-nitrogen-filled glovebox.

Crystal Growth. All single crystals examined in this study were grown from the melt by the Bridgman method. Doped crystals were prepared by adding Mn(II) (as $MnCl_2$) and/or Ni(II) (as $RbNiCl_3$) to the $RbMgCl_3$ prior to crystal growth. The samples were then sealed in evacuated Vycor ampules. The Bridgman apparatus has been previously described.[9] While low concentrations of Mn(II) produce no coloration, the presence of a small amount of Ni(II) imparts a noticeable color to the $RbMgCl_3$ crystals. Crystals which contain

(1) (a) Tulane University. (b) The University of Alabama.
(2) A. B. A. Schippers, V. Brandwijk, and E. W. Gorter, *J. Solid State Chem.*, **6**, 479 (1973).
(3) J. M. Longo and J. A. Kafalas, *J. Appl. Phys.*, **40**, 1601 (1969).
(4) J. M. Longo and J. A. Kafalas, *J. Solid State Chem.*, **1**, 103 (1969).
(5) J. M. Longo, J. A. Kafalas, N. Menyuk, and K. Dwight, *J. Appl. Phys.*, **42**, 1561 (1971).
(6) J. M. Longo and J. A. Kafalas, *J. Solid State Chem.*, **3**, 429 (1971).
(7) T. A. Tishura, G. N. Novitskaya, and A. N. Budarina, *Russ. J. Inorg. Chem.* (*Engl. Transl.*), **21**, 1613 (1976).
(8) H. J. Seifert and H. Fink, *Rev. Chim. Miner.*, **12**, 466 (1975).
(9) G. L. McPherson, L. J. Sindel, H. F. Quarls, and C. J. Doumit, *Inorg. Chem.*, **14**, 1831 (1975).

0020-1669/81/1320-0140$01.00/0

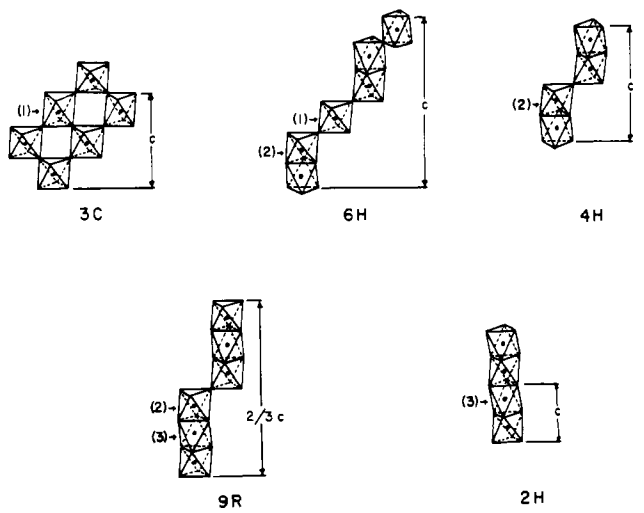

Figure 1. Schematic diagrams of the lattice types for the AMX_3 salts. The divalent metal ions are at the centers of the octahedra while the halide ions occupy the corners.

Table I. Unit Cell Data for 6H-, 4H-, and 9R-$RbMgCl_3$

hexagonal lattice	a, Å	c, Å	Z	ρ_o, g/cm^3	ρ_c, g/cm^3
6H-$RbMgCl_3$	7.095 (3)[a]	17.578 (5)[a]	6	2.77	2.81
4H-$RbMgCl_3$	7.10 [7.090][b]	11.84 [11.844][b]	4	2.76	2.78
9R-$RbMgCl_3$	7.10	26.85	9	2.75	2.75

[a] Numbers in parentheses represent the standard deviation in the last place of the reported parameter. [b] Numbers in brackets correspond to the values of Seifert and Fink in ref 8.

0.4–0.8 mol % Ni(II) (4H-$RbMgCl_3$) are pink while those with approximately 4 mol % Ni(II) (9R-$RbMgCl_3$) are yellow. In one of the Ni(II)-doped samples both the 4H and 9R phases appeared in the same ampule with a sharp line of demarcation. 4H-$RbMgCl_3$ was present in the upper portion of the sample while 9R-$RbMgCl_3$ occurred in the bottom portion. The bottom of the sample tube emerges from the Bridgman furnace first during the crystal growth.

Chemical Analyses. The nickel contents of two of the pink 4H-$RbMgCl_3$ crystals and one of the yellow 9R-$RbMgCl_3$ crystals were determined by Galbraith Laboratories, Inc., Knoxville, Tenn. The two 4H-$RbMgCl_3$ crystals were found to contain 0.4 and 0.8 mol % nickel while the 9R-$RbMgCl_3$ crystal contained 4 mol % nickel.

EPR Spectra. Crystals suitable for EPR study were selected from fragments obtained by breaking the larger crystals grown from the melt. The doped $RbMgCl_3$ crystals do not exhibit any prominent cleavage planes. The samples were oriented with the aid of a polarizing microscope and mounted so that the crystallographic c axis was contained in the plane of rotation of the magnetic field. The crystals were coated with "formvar" for protection from atmospheric moisture. The EPR spectra were recorded on a Varian E-3 X-band spectrometer using 100-kHz field modulation. Polycrystalline DPPH (diphenylpicrylhydrazyl) was used as a g-value reference ($g = 2.0036$).

Crystallographic Studies. Single crystals of all three phases of $RbMgCl_3$ were sealed in 0.3-mm glass capillaries and examined by X-ray diffraction. Precession photographs were taken by using filtered Mo Kα radiation. The initial studies indicated that the three materials crystallize in hexagonal lattices. The a dimensions of the three unit cells are nearly equal while the c dimensions differ dramatically. The densities of the materials were determined by flotation in $CCl_4/CHBr_3$ mixtures. A complete structural analysis of the 6H phase of $RbMgCl_3$ (undoped) was performed. A small crystal measuring 0.28 × 0.28 × 0.06 mm was chosen for data collection. Intensity measurements were collected on an Enraf-Nonius CAD-4 diffractometer equipped with a graphite monochromator. Accurate lattice parameters were determined by least-squares refinement of $((\sin\theta)/\lambda)^2$ value for 12 reflections with $\theta > 20°$. The lattice constants and densities of the three phases of $RbMgCl_3$ are presented in Table I.

The diffracted intensities were collected by using the ω–2θ scan technique with a takeoff angle of 3.5°. The scan rate was variable and was determined by a fast 20° min^{-1} prescan. Calculated speeds for the slow scan ranged from 20 to 0.3° min^{-1}. Moving crystal–moving counter backgrounds were collected for 25% of the total scan width at each end of the scan range. For each intensity the scan width was determined by

$$\text{scan range} = A + B \tan\theta$$

where $A = 0.80°$ and $B = 0.25°$. Aperture settings were determined in a similar manner with $A = 4$ mm and $B = 4$ mm. Other diffractometer parameters and the method of estimation of standard deviations have been described previously.[10] As a check on the stability of the instrument and the crystal, two reflections, $(20\bar{4})$ and $(0\bar{2}4)$, were measured after every 30 reflections; no significant variations were noted. One independent form of data was measured out to $2\theta = 50°$; a slow scan was performed on a total of 262 reflections. Since these data were scanned at a speed which would yield a net count of 4000, the calculated standard deviations were all very nearly equal. No reflection was subjected to a slow scan unless a net count of 50 was obtained in the prescan. The data were corrected for Lorentz, polarization, and absorption ($\mu = 117.5$ cm^{-1}) effects; the transmission factors varied from 0.07 to 0.48. This yielded a unique set of 249 observed reflections for *most* of these $I > 3\sigma(I)$.

The scattering factors for Mg^{2+}, Rb^+, and Cl^- were taken from the compilations of Cromer and Waber.[11] The scattering factor of Rb^+ was corrected for the real and imaginary components of anomalous scattering according to Cromer's table.[12] No corrections were made for extinction. Least-squares refinements were based on the minimization of $w(|F_o| - |F_c|)^2$; all calculations were carried out by using standard crystallographic programs.[13]

Refinement of the Structure. The systematic absences (hhl, $l \neq 2n$) of 6H-$RbMgCl_3$ are consistent with the space groups $P6_3/mmc$, $P6_3mc$, and $P\bar{6}c2$. It was assumed that 6H-$RbMgCl_3$ like $CsCdCl_3$ belonged to the centric space group $P6_3/mmc$. The unit cell contents of 6H-$RbMgCl_3$ in $P6_3/mmc$ are given in Table II. The initial atomic coordinates were taken from the structure of $CsCdCl_3$.[14] The positional parameters were refined along with isotropic thermal parameters to an R_1 of 0.112 (where $R_1 = [\sum(|F_o| - |F_c|)/\sum(F_o)]$). Anisotropic refinement led to final agreement indices of $R_1 = 0.070$ and $R_2 = 0.071$ ($R_2 = [\sum w(|F_o| - |F_c|)^2/\sum(F_o)^2]$). Unit weights were used at all stages of refinement, and unobserved reflections were not included. The largest parameter shifts in the final cycle of refinement were less than 0.1 of their estimated standard deviations. The positional and thermal parameters are given in Table III.

Table II. Unit Cell Contents of 6H-$RbMgCl_3$[a]

atom	Wyckoff designatn	point sym	coordinates	no. of positns
Rb(1)	(b)	$\bar{6}m2$	0, 0, 1/4	2
Rb(2)	(f)	$3m$	1/3, 2/3, z	4
Mg(1)	(a)	$\bar{3}m$	0, 0, 0	2
Mg(2)	(f)	$3m$	1/3, 2/3, z	4
Cl(1)	(h)	mm	x, $2x$, 1/4	6
Cl(2)	(k)	m	x, $2x$, z	12

[a] Based on space group $P6_3/mmc$.

Results and Discussion

Three Lattice Types of $RbMgCl_3$. In general the unit cell constants are sufficient to determine the lattice type of an AMX_3 salt. From the data in Table I it is clear that undoped $RbMgCl_3$ prepared in *our* laboratories adopts lattice type 6H while $RbMgCl_3$ with 0.4–0.8 mol % Ni(II) and $RbMgCl_3$ with 4 mol % Ni(II) crystallize in lattice types 4H and 9R, respectively (see Figure 1). The densities indicate that the

(10) J. L. Atwood and K. D. Smith, *J. Am. Chem. Soc.*, **95**, 1488 (1973).
(11) D. T. Cromer and J. T. Waber, *Acta Crystallogr.*, **18**, 104 (1965).
(12) D. T. Cromer, *Acta Crystallogr.*, **18**, 17 (1965).
(13) Crystallographic programs used on a UNIVAC 1110 included ORABS (absorption correction, by Busing, Levy, and Wehe), ORFLS (structure factor calculation and least-squares refinement, by Busing, Martin, and Levy), ORFFE (distances and angles with esd's by Busing, Martin, and Levy), and ORTEP (thermal ellipsoid drawings, by C. K. Johnson).
(14) J. R. Chang, G. L. McPherson, and J. L. Atwood, *Inorg. Chem.*, **14** 3079 (1975).

Table III. Positional and Thermal Parameters[a]

atom	x/a	y/b	z/c	β_{11}	β_{22}	β_{33}	β_{12}	β_{13}	β_{23}
Rb(1)	0	0	1/4	0.0127 (17)	0.0127	0.0024 (2)	0.0064	0.0000	0.0000
Rb(2)	1/3	2/3	0.0896 (2)	0.0120 (10)	0.0120	0.0027 (1)	0.0060	0.0000	0.0000
Mg(1)	0	0	0	0.0098 (50)	0.0098	0.0009 (5)	0.0049	0.0000	0.0000
Mg(2)	1/3	2/3	0.8403 (6)	0.0079 (30)	0.0079	0.0012 (4)	0.0040	0.0000	0.0000
Cl(1)	0.5090 (12)	1.0172	1/4	0.0118 (16)	0.0057 (17)	0.0015 (2)	0.0028	0.0000	0.0000
Cl(2)	0.8339 (10)	1.6677	0.0816 (3)	0.0163 (13)	0.0081 (13)	0.0024 (2)	0.0040	0.0010	0.0019 (4)

[a] Anisotropic temperature factors of the form $\exp[-(\beta_{11}h^2 + \beta_{22}k^2 + \beta_{33}l^2 + 2\beta_{12}hk + 2\beta_{13}hl + 2\beta_{23}kl)]$. The following constraints are placed on the thermal parameters: for Rb(1), Rb(2), Mg(2), and Mg(2), $\beta_{11} = \beta_{22} = 2\beta_{12}$, $\beta_{13} = \beta_{23} = 0$; for Cl(1), $\beta_{22} = 2\beta_{12}$, $\beta_{13} = \beta_{23} = 0$; for Cl(2), $\beta_{22} = 2\beta_{12}$, $2\beta_{13} = \beta_{23}$.

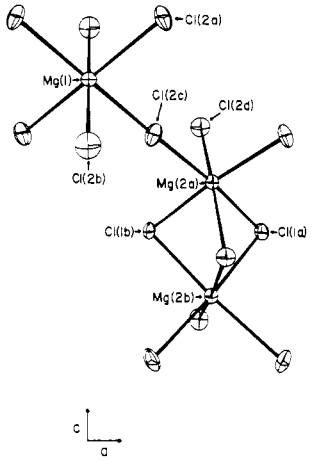

Figure 2. ORTEP drawing of a portion of the structure of 6H-$RbMgCl_3$ which shows the coordination spheres of the two types of magnesium ions.

packing efficiences of the different lattice types are approximately the same, although there is a small but noticeable decrease in both the observed and calculated densities from 6H-$RbMgCl_3$ to 4H-$RbMgCl_3$ to 9R-$RbMgCl_3$. This small decrease in density is consistent with the pressure studies of Longo and Kafalas which determined that corner-shared octahedral structures pack somewhat more efficiently than face-shared structures.[3-6] The fraction of corner-shared $MgCl_6^{4-}$ complexes in $RbMgCl_3$ is greatest in the 6H phase and smallest in the 9R phase. It appears that the addition of Ni(II) to $RbMgCl_3$ has an effect which is just the opposite of that produced by the application of high pressure. For example, $CsMnCl_3$ undergoes a series of lattice transformations under increasing pressure where the low-pressure form, lattice type 9R, is converted first to 4H, then to 6H, and finally to 2H.[6]

Structure of 6H-$RbMgCl_3$. The X-ray determination shows that 6H-$RbMgCl_3$ adopts a structure very similar to those of $CsCdCl_3$[14] and $RbMnCl_3$.[15] The interatomic distances and angles calculated from the analysis of $RbMgCl_3$ are given in Table IV. In terms of the EPR spectra, the most important structural features are the environments of the two crystallographically distinct magnesium ions. Figure 2 shows an ORTEP drawing of the coordination spheres of one Mg(1) ion and two Mg(2) ions. The six chloride ions (Cl(2)) which surround Mg(1) are equivalent and form an octahedron which is regular within experimental error. Within 1 standard deviation the Cl(2a)–Cl(2b) distance is equal to the Cl(2b)–Cl(2c) distance, and the Cl(2a)–Mg(1)–Cl(2b) and Cl(2b)–Mg(1)–Cl(2c) angles are equal to 90°. The octahedron containing Mg(1) joins corners with six octahedra containing Mg(2) ions, forming Mg(1)–Cl(2)–Mg(2) bridges that are nearly linear. Each of the octahedra containing Mg(2) ion also shares a face with a second Mg(2)-containing octahedron, forming three bent Mg(2)–Cl(1)–Mg(2) bridges. Thus, the coordination sphere of each Mg(2) ion contains two distinct groups of chloride ions (Cl(1) and Cl(2)) which have significantly different Mg–Cl distances. Presumably, the electrostatic repulsion between the two Mg(2) ions causes the Mg(2)–Cl(1) distances to lengthen relative to the Mg(2)–Cl(2) distances (2.507 compared with 2.470 Å). In contrast to the environment of Mg(1), the coordination sphere of Mg(2) is noticeably distorted from that of a regular octahedron. The rigorous site symmetry at Mg(1) is D_{3d} while that at Mg(2) is C_{3v}. In both sites the threefold axis is parallel to the crystallographic *c* axis.

Table IV. Selected Interatomic Distances and Angles

atoms[a]	dist,[b] Å		atoms	dist, Å
Mg(2a)–Mg(2b)	3.175 (20)	{3.168}	Rb(2)–Cl(2)	3.547 (4)
Mg(1)–Cl(2)	2.494 (6)		Cl(1a)–Cl(1b)	3.358 (8)
Mg(2)–Cl(1)	2.507 (9)	{2.48}	Cl(1b)–Cl(2c)	3.571 (5)
Mg(2)–Cl(2)	2.470 (8)	{2.47}	Cl(2a)–Cl(2b)	3.520 (9)
Rb(1)–Cl(1)	3.544 (4)		Cl(2b)–Cl(2c)	3.533 (11)
Rb(1)–Cl(2)	3.595 (6)		Cl(2c)–Cl(2d)	3.556 (11)
Rb(2)–Cl(1)	3.548 (5)			

atoms	angle, deg	atoms	angle, deg
Cl(2a)–Mg(1)–Cl(2b)	89.8 (2)	Cl(2c)–Mg(2a)–Cl(2d)	92.1 (3) {91.6}
Cl(2b)–Mg(1)–Cl(2c)	90.2 (2)	Mg(2a)–Cl(1a)–Mg(2b)	78.6 (4) {79.8}
Cl(1a)–Mg(2a)–Cl(1b)	84.2 (3) {84.1}	Mg(1)–Cl(2c)–Mg(2a)	178.7 (3)
Cl(1a)–Mg(2a)–Cl(2d)	91.7 (2)		

[a] Atom designations refer to Table II and Figure 2. [b] The numbers in parentheses are the standard deviations in the last decimal place of the reported parameters. The numbers in brackets are taken from the structure of Seifert and Fink in ref 8.

It is interesting to note that the dimeric unit formed by the two Mg(2)-containing octahedra is structurally similar to the $Mg_2Cl_9^{5-}$ units of 4H-$RbMgCl_3$. The corresponding interatomic distances and angles for the $Mg_2Cl_9^{5-}$ moiety in 4H-$RbMgCl_3$ determined by Seifert and Fink are included in Table IV for comparison. The structural data indicate that the geometries of the $Mg_2Cl_9^{5-}$ units are nearly identical in the two structures. This conclusion is quite consistent with the EPR studies described in the next section.

EPR Spectra of Doped $RbMgCl_3$ Crystals. There are three structurally distinct types of divalent ion sites which can occur in the AMX_3 crystals. In one type a MX_6^{4-} complex shares corners with six other MX_6^{4-} complexes. In Figure 1 sites of this type are designated by (1). In the second type, designated by (2), an MX_6^{4-} complex shares a face and three corners with neighboring MX_6^{4-} complexes. In the third type of site, (3), an MX_6^{4-} complex shares opposite faces with two other MX_6^{4-} complexes. Two types of magnesium ion sites occur in 6H-$RbMgCl_3$ and 9R-$RbMgCl_3$, while 4H-$RbMgCl_3$ contains only one magnesium ion site. In all three lattices the EPR spectra of paramagnetic impurities which have substituted for

(15) J. Goodyear, G. A. Steigmann, and E. M. Ali, *Acta Crystallogr., Sect. B, B33*, 256 (1977).

Table V. Spin Hamiltonian Parameters

ion	lattice	site	$g_\parallel$	$g_\perp$	A, cm^{-1}	B, cm^{-1}	D, cm^{-1}	$\lvert a - F\rvert$, cm^{-1}
Mn(II)[a]	6H-$RbMgCl_3$	1	2.00	2.00	±0.0083	±0.0083	∓0.0099	0.0001
		2	2.00	2.00	±0.0083	±0.0083	∓0.0122	0.0001
	4H-$RbMgCl_3$	1	2.00	2.00	±0.0083	±0.0083	∓0.0123	0.0001
	9R-$RbMgCl_3$	2	2.00	2.00	±0.0083	±0.0083	∓0.0123	0.0001
		3	2.00	2.00	±0.0079	±0.0079	∓0.0266	0.0001
	$CsMgCl_3$[b]	3	2.00	2.00	±0.0080	±0.0080	∓0.0303	
Ni(II)[c]	4H-$RbMgCl_3$	2	2.28	2.28			∓0.854	

[a] Room temperature. [b] Taken from ref 18. [c] Liquid-nitrogen temperature.

magnesium ions should exhibit axial symmetry about the crystallographic c axis.

The EPR spectrum of Mn(II) in an axially symmetric environment can be described by the spin Hamiltonian

$$\mathcal{H} = g_\parallel \beta H_z \hat{S}_z + g_\perp \beta (H_x \hat{S}_x + H_y \hat{S}_y) + A \hat{I}_z \hat{S}_z + B(\hat{I}_x \hat{S}_x + \hat{I}_y \hat{S}_y) + D[\hat{S}_z^2 - \tfrac{1}{3}(S(S+1))] + \text{higher order terms}$$

The first two terms account for the electron Zeeman interaction, while the second two terms describe the hyperfine interaction associated with the nucleus of the central metal ion. The remaining terms treat the zero-field field splitting which results from the coupling of the axial ligand field with the many electron ($S = {}^5/_2$) ion. The higher order zero-field field effects are very small in the case of Mn(II) in $RbMgCl_3$. The actual terms are given in a number of standard references.[16] Usually, the spin Hamiltonian parameters can be measured directly from the spectra observed when the magnetic field is either parallel or perpendicular to the crystallographic c axis. The manganese resonances are well resolved at room temperature in all three phases of $RbMgCl_3$.

In 6H-$RbMgCl_3$ there appear to be two distinct manganese resonances, corresponding to two different sites in the host lattice. The fine and hyperfine structures from these two manganese ions overlap extensively. For high-spin Mn(II), the axial field splitting of the $S = {}^5/_2$ system leads to a five-line fine structure while the interaction with the ^{55}Mn nucleus ($I = {}^5/_2$) splits each line into six. This gives a total of 30 allowed lines for each kind of Mn(II) ion. Because of the extensive overlap, the spectral analysis was carried out with the aid of computer simulations. The simulated spectra correspond to the composite shape resulting from the combination of the 60 allowed lines from two inequivalent, axially symmetric Mn(II) ions. The relative intensities of the lines arising from different fine structure components were fixed at the theoretical ratios of 5:8:9:8:5. These ratios assume that the intensity of an allowed EPR absorption is proportional to $|\langle S,m|\hat{S}_+|S,m-1\rangle|^2$. Each line was given a width of 12 G (peak to peak) and a shape which is 20% Gaussian and 80% Lorentzian. The resonance fields were calculated from the perturbation solutions derived by Bleaney for the axial spin Hamiltonian.[17] The intensities of the two manganese resonances relative to each other were varied along with the parameters for the two Mn(II) ions until a satisfactory agreement between the observed and calculated spectra was obtained. Both the parallel ($\theta = 0°$) and perpendicular ($\theta = 90°$) spectra were analyzed in this fashion. The angle θ is taken as the angle between the magnetic field and the crystallographic c axis. The best agreement is obtained when the two manganese resonances are given approximately equal intensities. Figure 3 shows a comparison of the observed and calculated parallel spectra for 6H-$RbMgCl_3$; the simulation is based on the spin Hamiltonian parameters in Table V. The agreement is quite good in the outer portions of the spectrum, but there are small discrepancies in the center. Although numerous simulations were made, it was not possible to obtain an exact fit. The explanation for the minor discrepancies is not clear. The overall agreement between the observed and simulated spectra is noticeably better for the perpendicular orientation ($\theta = 90°$). The spin Hamiltonian parameters obtained in the analysis are quite reasonable for Mn(II) in a chloride lattice. It is unlikely that the true values of these parameters differ significantly from those given in Table V. Certainly, there is no doubt that there are two distinct types of Mn(II) ions which are present in approximately equal concentrations. Apparently the Mn(II)

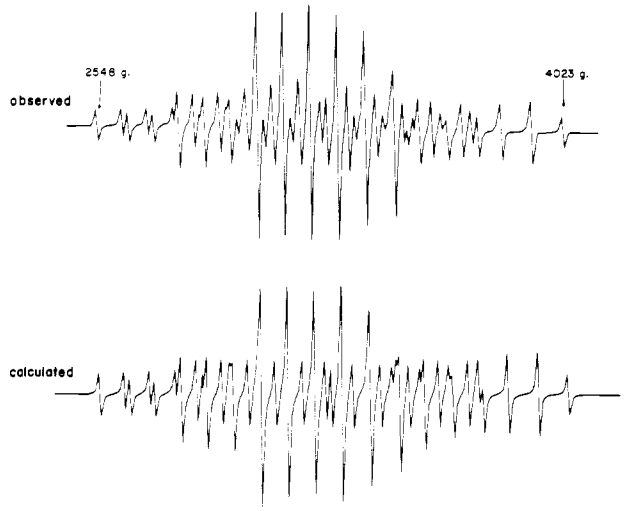

Figure 3. EPR spectrum of 6H-$RbMgCl_3$ doped with Mn(II) recorded at room temperature with the magnetic field parallel to the crystallographic c axis. The calculated spectrum was obtained by using the parameters given in Table V.

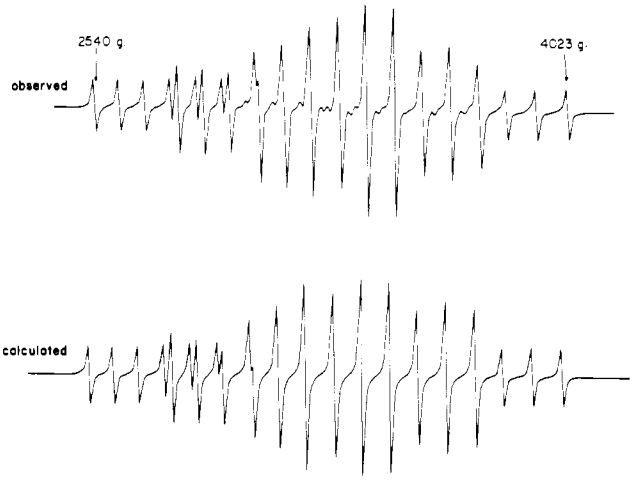

Figure 4. EPR spectrum of 4H-$RbMgCl_3$ doped with Mn(II) recorded at room temperature with the magnetic field parallel to the crystallographic c axis. The calculated spectrum was obtained by using the parameters in Table V.

(16) See for example, A. Abragam and B. Bleaney, "Electron Paramagnetic Resonance of Transition Metal Ions", Oxford University Press, London, 1970, p 437.
(17) B. Bleaney, *Philos. Mag.*, **42**, 441 (1951).

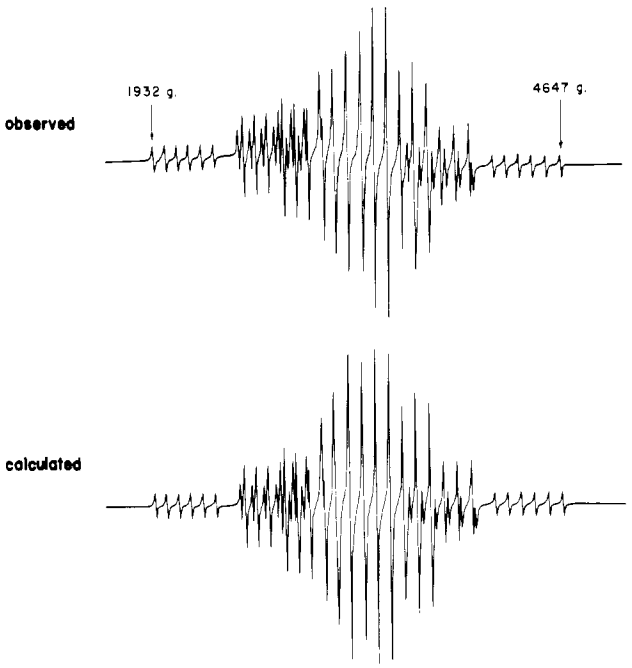

Figure 5. EPR spectrum of 9R-$RbMgCl_3$ doped with Mn(II) recorded at room temperature with the magnetic field parallel to the crystallographic *c* axis. The calculated spectrum was obtained by using the parameters in Table V.

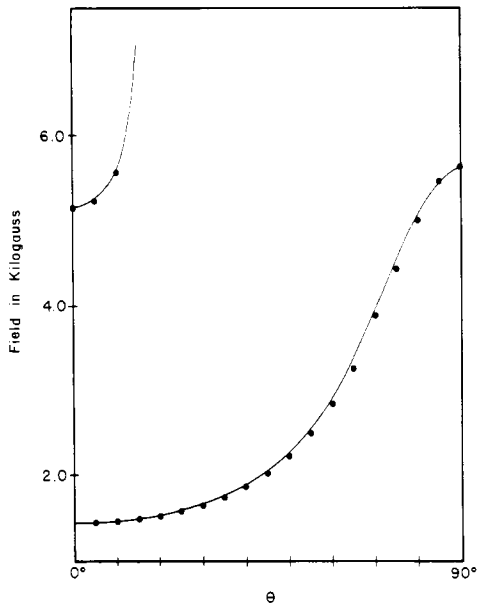

Figure 6. Angular dependence of the Ni(II) resonance in 4H-$RbMgCl_3$ recorded at 77 K. The resonance fields are plotted on the vertical axis while the θ values (θ is the angle between the magnetic field and the crystallographic *c* axis) are shown on the horizontal axis. The dots represent the observed resonance fields. The solid curves were calculated from the parameters in Table V.

ions readily enter both magnesium sites in 6H-$RbMgCl_3$.

EPR analysis of the 4H and 9R phases proceeded in a similar fashion. The observed and calculated room temperature spectra for 4H-$RbMgCl_3$ and 9R-$RbMgCl_3$ are seen in Figures 4 and 5, respectively. The appropriate spin Hamiltonian parameters are shown in Table V. The simulation for 4H-$RbMgCl_3$ assumes that there is only one type of Mn(II) ion present in the crystal. This is consistent with the structure of the 4H phase. In 9R-$RbMgCl_3$ there are two magnesium sites and the EPR spectrum clearly shows two distinct manganese resonances. The best fit results when the intensity of the resonance with the smaller zero-field splitting is taken to be approximately 3 times that of the resonance with the larger zero-field splitting. For both 4H- and 9R-$RbMgCl_3$ the agreement between the observed and calculated spectra is quite good.

From the spin Hamiltonian parameters, it is possible to assign each of the manganese resonances which appear in 6H-$RbMgCl_3$ and 9R-$RbMgCl_3$ to particular magnesium sites in the two host lattices. The axial component of the zero-field splitting is the most sensitive of the magnetic properties to the structural characteristics of the Mn(II) ion environment. In both 6H-$RbMgCl_3$ and 9R-$RbMgCl_3$ the zero-field field splitting parameter (D) of one of the two manganese resonances is nearly identical with that of Mn(II) in 4H-$RbMgCl_3$ (see Table V). The other spin Hamiltonian parameters for these three Mn(II) ions are also in close agreement. This suggests that there is one magnesium site which has nearly the same structure in all three phases. It seems almost certain that the three manganese resonances which have such similar magnetic properties must arise from Mn(II) ions in type 2 sites (see Figure 1). In 9R-$RbMgCl_3$ the second resonance must correspond to Mn(II) ions in the site with two shared faces, type 3. This site is similar to the magnesium site in $CsMgCl_3$. The EPR spectrum of Mn(II) in $CsMgCl_3$ has already been studied,[18] and the spin Hamiltonian parameters are included in Table V. The resemblance between the second manganese resonance in 9R-$RbMgCl_3$ and the manganese resonance in $CsMgCl_3$ adds additional support to the validity of the assignments in Table V. It is interesting to note that, even though a second paramagnetic ion, Ni(II), is present in the 4H- and 9R-$RbMgCl_3$ crystals (4 mol % in 9R-$RbMgCl_3$), the Mn(II) resonance are quite sharp with no evidence of manganese–nickel interactions. In terms of the manganese impurities, the materials behave as completely diamagnetic host lattices.

When 4H-$RbMgCl_3$ is cooled to 77 K, a nickel resonance appears which is resolved well enough for an analysis. The spectrum can be described by the relatively simple axial spin Hamiltonian

$$\mathcal{H} = g_{\parallel}\beta H_z\hat{S}_z + g_{\perp}\beta(H_x\hat{S}_x + H_y\hat{S}_y) + D[\hat{S}_z^2 - \tfrac{1}{3}S(S+1)]$$

The exact rather than perturbation solutions to this Hamiltonian were used to fit the spectrum since the magnitude of the zero-field splitting is quite large. Exact solutions were obtained by computer diagonalization of the three-by-three Hamiltonian matrix. The spectrum was fit as a function of crystal orientation (see Figure 6). The agreement between the observed behavior and the behavior calculated from the parameters in Table V is excellent. When 9R-$RbMgCl_3$ (4 mol % Ni(II)) is cooled to 77 K, a nickel resonance appears but is very broad and poorly resolved. There is some evidence that the crystals undergo a phase transition between room and liquid-nitrogen temperature in which the axial symmetry of the lattice is lost. The spectrum of this material was not pursued further.

Structural Chemistry of $RbMgCl_3$. Among the AMX_3 salts, $RbMgCl_3$ appears unique in the sense that relatively minor variations in chemical composition are sufficient to produce dramatic structural changes. This is the first occasion in our spectroscopic studies of doped AMX_3 crystals that the introduction of an impurity at the level of one part in 200 has caused the host material to crystallize in a different lattice. Although the data presented here do not provide a quantitative relationship between the concentration of Ni(II) impurity and the structure adopted by the doped material, the qualitative

(18) G. L. McPherson, T. J. Kistenmacher, and G. D. Stucky, *J. Chem. Phys.*, **52**, 815 (1970).

aspects are clear. As the concentration of nickel is increased, the material crystallizes in lattices with progressively greater fractions of face-shared octahedral structures. One would expect that ultimately a 2H lattice would be adopted since pure $RbNiCl_3$ has the 2H structure. At this time we have no estimate of the minimum concentration of nickel necessary to produce a 2H phase. It is possible, however, that magnesium ion has only a limited solubility in a 2H lattice. Other divalent ions such as V(II) and Co(II) which have 2H-$RbMCl_3$ structures might be expected to produce structural modifications in $RbMgCl_3$ similar to those caused by Ni(II). The fact that Mn(II) does not cause lattice modifications seems reasonable since pure $RbMnCl_3$ adopts a 6H structure.

The EPR spectra clearly show that Mn(II) impurities readily enter both magnesium sites in 4H- and 9R-$RbMgCl_3$. The relative intensities, however, indicate that the distribution of Mn(II) ions between the two sites is not precisely statistical. In 6H-$RbMgCl_3$ there are two type 2 sites for each type 1 site, but the Mn(II) concentration in types 1 and 2 appear to be nearly equal. In 9R-$RbMgCl_3$ there are two type 2 sites for each type 3 site, but the Mn(II) concentration in type 2 is approximately 3 times that in type 3. Although the Mn(II) ions discriminate between sites, the level of selectivity is relatively small. This observation is consistent with earlier studies on doped $CsCdCl_3$ crystals where Mn(II) was found to be less selective with respect to different lattice sites than either V(II) or Ni(II).[14]

Finally, it should be noted that the 2H phase of $RbMgCl_3$ reported by Tishura and co-workers[7] was never encountered in our investigations. There is some indication that the material which they characterized actually had a 4H or 6H structure. The lattice constant reported for the *c* axis is 5.936 Å which is smaller than the *c* axis of $CsMgCl_3$, 6.187 Å,[18] by more than 0.2 Å. If the lattice constants of a number of known 2H lattices ($CsVCl_3$, $RbVCl_3$, $CsCoCl_3$, $RbCoCl_3$, $CsNiCl_3$, $RbNiCl_3$)[19-22] are considered, it appears that the *c* dimensions of the rubidium salts are only about 0.03 Å smaller than those of the corresponding cesium salts. The value of 5.936 Å is almost exactly one-half of the *c* dimension of 4H-$RbMgCl_3$ and one-third of the *c* dimension of 6H-$RbMgCl_3$. It is possible that Tishura and co-workers did not properly index the X-ray powder pattern from the $RbMgCl_3$ which they prepared.

Registry No. $RbMgCl_3$, 40611-15-2; Mn, 7439-96-5; Ni, 7440-02-0.

Supplementary Material Available: A list of structure factors for 6H-$RbMgCl_3$ (3 pages). Ordering information is given on any current masthead page.

(19) R. W. Asmussen, T. K. Larsen, and H. Soling, *Acta Chem. Scand.*, **23**, 2055 (1969).
(20) H. J. Seifert and P. Ehrlich, *Z. Anorg. Allg. Chem.*, **302**, 284 (1959).
(21) H. Soling, *Acta Chem. Scand.*, **22**, 2793 (1968).
(22) A. Engberg and H. Soling, *Acta Chem. Scand.*, **21**, 168 (1967).
(23) G. N. Tischenko, *Tr. Inst. Kristallogr., Akad. Nauk SSSR*, **11**, 93 (1955).

Contribution from Ames Laboratory—DOE and Department of Chemistry, Iowa State University, Ames, Iowa 50011

Synthesis by Hydrogen-Driven Disproportionation Reactions. Synthesis and Structure of the Hexazirconium Dodecahalide Clusters Zr_6Cl_{12} and Zr_6Br_{12} and the Double Salt $Zr_6Cl_{12}{\cdot}M_2ZrCl_6$ (M = Na, K, Cs)

HIDEO IMOTO, JOHN D. CORBETT,* and ALAN CISAR

Received February 6, 1980

The ZrXH phases, X = Cl, Br, formed by reaction of H_2 with double-metal-layered ZrX at 150–450 °C are metastable and decompose at 630–780 °C to ZrH_2 plus the cluster compound Zr_6X_{12}, the latter being isostructural with Zr_6I_{12}. Transport of Zr_6Cl_{12} occurs in the sealed Ta container at about 800 °C. The two cluster phases are also formed as powders from incomplete reactions of ZrX and ZrX_4 at 650–700 °C, while the layered 3R-$ZrCl_2$ is more stable at lower temperatures. Decomposition of ZrClH in the presence of NaCl, KCl, or CsCl at 750 °C yields the isostructural $M_2Zr_7Cl_{18}$ (M = Na, K, Cs) while ZrCl does not react with NaCl or KCl alone under the same conditions. The crystal structure of the double salt $K_2Zr_7Cl_{18}$ was solved by single-crystal diffractometer methods ($R\bar{3}$, a = 9.499 (2) Å, c = 25.880 (6) Å, R = 0.037, R_w = 0.049, 736 Mo Kα diffractions corrected for absorption). The structure contains the octahedral metal cluster Zr_6Cl_{12} slightly compressed along the $\bar{3}$ axis [d(Zr–Zr) = 3.224 (1), 3.178 (1) Å] and edge bridged by chlorine. Halides in octahedral $ZrCl_6^{2-}$ groups occupy all exo positions of the clusters. The structure can also be described in terms of nine chlorine layers per cell containing regular potassium and vacancy substitutions together with zirconium(II) and zirconium(IV) in octahedral interstices. The Zr_6Cl_{12} and $Na_2Zr_7Cl_{18}$ phases quenched in the presence of hydrogen at ~1 atm do not contain hydrogen in the clusters.

Introduction

Zirconium monochloride and monobromide provided the first two examples of a new and novel structure type, namely, infinite sheets of strongly bonded double-metal layers sandwiched between double-halogen layers,[1-3] the structures of ZrCl and ZrBr differing only in packing details of the four-layer slabs. The zirconium monohalides were subsequently both found to react with hydrogen quite readily to form distinct hemihydride and monohydride phases,[4] and the magnitudes of the enthalpy changes for these reactions together with chemical reasoning suggested that the strongly bound hydrogen is located in the electron-rich region between the double-metal layers. Subsequent NMR studies[5,6] have indicated that the hydrogen is probably distributed principally among the tetrahedral interstices between the metal layers.

The initial motivation for the present research came from a desire to grow single crystals of $ZrXH_{0.5}$ (X = Cl, Br). Although the heavy-atom positions in $ZrXH_{1.0}$ have recently been deduced from X-ray powder data,[7] it has not been possible to solve the lower symmetry structure of the hemihydride

(1) Troyanov, S. I. *Vestn. Mosk. Univ., Ser. 2: Khim.* **1973**, *28*, 369.
(2) Adolphson, D. G.; Corbett, J. D. *Inorg. Chem.* **1976**, *15*, 1820.
(3) Daake, R. L.; Corbett, J. D. *Inorg. Chem.* **1977**, *16*, 2029.
(4) Struss, A. W.; Corbett, J. D. *Inorg. Chem.* **1977**, *16*, 360.
(5) Hwang, T. Y.; Torgeson, D. R.; Barnes, R. G. *Phys. Lett. A* **1978**, *66A*, 137.
(6) Murphy, P. D.; Gerstein, B. C. *J. Chem. Phys.* **1979**, *70*, 4552.
(7) Daake, R. L.; Corbett, J. D., unpublished research.

0020-1669/81/1320-0145$01.00/0